Antioxidants and Redox Signaling

DOI: 10.1089/ars.2020.8059

Original Research Communication

Mitochondria as Target for Tumor Management of Hemangioendothelioma

Gayle M Gordillo[1*¶], Ayan Biswas[1¶], Kanhaiya Singh[1], Abhishek Sen[1], Poornachander R Guda[1], Caroline Miller[4], Xueliang Pan[3], Savita Khanna[1], Enrique Cadenas[5] and Chandan K Sen[1,2]

1. Indiana Center for Regenerative Medicine & Engineering, Indiana University Health Comprehensive Wound Center, Department of Surgery, Indiana University School of Medicine, Indianapolis, IN 46202
2. Department of Surgery, The Ohio State University, Columbus, OH 43210.
3. Department of Biomedical Informatics, The Ohio State University, Columbus, OH 43210
4. Electron microscopy core, Indiana University School of Medicine, Indianapolis, IN 46202
5. Pharmacology & Pharmaceutical Sciences, School of Pharmacy, University of Southern California, Los Angeles, CA, 90089,

[¶] These authors contributed equally to this work

***Corresponding Author**

Professor Gayle M Gordillo

Indiana Center for Regenerative Medicine & Engineering, Department of Surgery, Indiana University School of Medicine, Indianapolis, IN 46202

Tel.: +1 317-944-3636

E-mail: gmgordil@iu.edu

Abbreviated title: *Mitochondria as Target for the Management of HE*

Word count: 4124

Reference number: 65

Number of color illustrations: online 8 and hardcopy 8

KEYWORDS: Hemangioendothelioma, Mitochondria, Radiation, Tumor, Therapy.

List of abbreviations:

HE : Hemangioendothelioma

EOMA : Mouse Hemangioendothelioma Endothelial Cells.

MAE : mouse aortic endothelial cells.

XRT : X-ray therapy

NBE : Natural berry extract

FDA : Food and Drug Administration

IND : Investigational New Drug

NIOSH : National Institute for Occupational Safety and Health

ATP : Adenosine triphosphate

OCR : Oxygen consumption rate

ECAR : extracellular acidification rate

Drp1 : Dynamin-related protein

Mfn2 : Mitofusin 2

SIRT3 : sirtuin-3

AMPK : AMP-activated *protein* kinase

DMSO : Dimethyl sulfoxide

DMEM : Dulbecco's Modified Eagle Medium

FBS : Fetal bovine serum

PGC-1α: proliferator-activated receptor-γ coactivator-1α

Antioxidants and Redox Signaling
Mitochondria as Target for Tumor Management of Hemangioendothelioma (DOI: 10.1089/ars.2020.8059)

Antioxidants and Redox Signaling
Mitochondria as Target for Tumor Management of Hemangioendothelioma (DOI: 10.1089/ars.2020.8059)

Abstract:

Aims: Hemangioendothelioma (HE) may be benign or malignant. EOMA cells are validated to study mechanisms in HE. This work demonstrates that EOMA cells heavily rely on mitochondria to thrive. Thus, a combination therapy including weak X-ray therapy (XRT, 0.5Gy) and a standardized natural berry extract (NBE) that is known to be effective in managing experimental HE and has been awarded with Food and Drug Administration - Investigational New Drug Application (FDA-IND # 140318) for studies on infantile hemangioma was tested.

Results: NBE treatment alone selectively attenuated basal oxygen consumption rate (OCR) of EOMA cells. NBE significantly sensitized EOMA, but not MAE, cells to XRT-dependent attenuation of mitochondrial respiration and ATP production. Combination treatment selectively and potently influenced mitochondrial dynamics in EOMA cells such that fission was augmented. Markers of mitochondrial fission were induced by the said combination therapy. This was achieved by lowering of mitochondrial Sirtuin 3 (SIRT3) causing increased phosphorylation of AMP-activated protein kinase (AMPK). A key role of SIRT3 in loss of EOMA cell viability caused by the combination therapy was evident when pyrroloquinoline quinone, an inducer of SIRT3, pre-treatment rescued these cells.

Innovation and Conclusion: Mitochondria-targeting NBE significantly extended survival of HE-affected mice. The beneficial effect of combination therapy was, however, far more potent with 3-fold increase in murine survival. Mitochondria-targeted antitumor therapies warrant further consideration.

Introduction:

Clinically presented as vascular neoplasms, hemangioendothelioma (HE) may also display characteristics intermediate between entirely benign hemangiomas and highly malignant angiosarcomas (38,59,63). In children, they frequently cause deformity and can cause death. Kaposiform hemangioendothelioma features several solid poorly circumscribed nodules such that each nodule is composed of a mixture of small capillaries and solid lobules of endothelial cells arranged in a glomeruloid pattern. EOMA cells are a validated experimental model to study mechanisms in HE and its management (11,12,23).

Mitochondrial functionality is a critical requirement for tumor anabolism. The growth of neoplastic tissue is supported by a hyperactive glycolytic machinery, often anaerobic. It is commonly accepted that pyruvate, thus generated in the cytoplasm, is shunted to produce lactate via lactate dehydrogenase. It has been thus assumed that tumor cells are limited in their capacity for oxidative phosphorylation (OXPHOS). Such notion would assign low value to mitochondrial functionality for its significance in supporting tumor anabolism(51) . More recent work, however, appreciates that tumor metabolism is less homogenous than was previously imagined (51). Thorough characterization of the metabolic process involved in tumor has now identified tumorigenic cell populations that are heavily reliant on mitochondrial respiration compared to their dependence on glycolysis. Mitochondrial depletion of cancer cells markedly limited tumorigenic potential (13,25,37,60). Loss of mitochondrial respiration causes proliferating cancer cells to become functionally limited for electron acceptors(50) .

Recent literature suggest an essential role of mitochondria in cancer. Cancer cells devoid of mitochondrial DNA (mtDNA) lose tumorigenic potential unless OXPHOS is reconstituted in these cells by mitochondria acquired from host stroma (7). Furthermore, defects in OXPHOS sensitized tumor cells to cytotoxic drugs (13,53). Conventional radiation therapy is known to compromise tumor mitochondrial function (44). Targeting mitochondrial function has emerged as a viable strategy for the development of novel anticancer agents. Cytotoxic drugs, the cornerstone for chemotherapy, however, are notorious for their adverse side effects. Furthermore, many of these cytotoxic drugs are classified by National

Institute for Occupational Safety and Health (NIOSH) as hazardous drugs as they threaten the health of an estimated 8 million U.S. healthcare workers.

Berry polyphenols have been recognized for their chemopreventive properties (40,52). Low fruit and vegetable intake is a known contributor to cancer related deaths (5,58). On the other hand, specific phytochemicals such as anthocyanins are known to act on a number of specific molecular mechanisms that inhibit tumorigenesis (56). Our recent work has identified that a standardized anthocyanin-rich natural berry extract (NBE) is effective in prolonging survival of HE bearing mice (11). The objective of this work is to investigate tumor mitochondrial function and its significance in the development of HE as well as in the survival of HE-bearing mice. NBE and therapeutic gamma X-ray radiation (XRT) have been tested, alone or together in low dosages to study potential interaction, for their ability to target mitochondrial respiration in tumor cells.

Results:

Sensitization of tumor forming endothelial cells to effects of XRT is time and dose dependent. To determine the dose and duration of NBE and XRT exposure, cell toxicity studies were performed. The NBE dose (200 μg/ml) and pre-treatment duration were determined using previously reported toxicity and dose response studies for EOMA cells (4). Non-tumor forming murine aortic endothelial (MAE) cells were used as controls (11,12).Time and dose responses to XRT were analyzed using LDH and PI exclusion assays to identify the threshold dose of XRT needed to induce cell toxicity (**Figs. 1a-b**). XRT dose with 1.0 Gy (24h) was toxic in MAE cells (**Fig 1a**). This toxicity was, however, not observed using LDH leakage assay (**Fig 1b**) which is known to be less sensitive than flow-cytometry based PI assay (15). EOMA cells, on the other hand, were sensitive to NBE treatment alone (**Fig. 1a-b**), as demonstrated by both PI exclusion as well as LDH leakage assays. Interestingly, NBE pretreatment sensitized EOMA cells to weak XRT (0.5Gy) mediated toxicity. Since weak XRT alone in EOMA cells did not induce toxicity, NBE pretreatment followed by a regimen of weak XRT was selected as the threshold condition to induce cell toxicity in EOMA cells as this treatment regimen was non-toxic for healthy MAE cells (**Fig. 1a-b**).

Antioxidants and Redox Signaling
Mitochondria as Target for Tumor Management of Hemangioendothelioma (DOI: 10.1089/ars.2020.8059)

NBE sensitized EOMA, not MAE, cells to weak XRT by inhibiting mitochondrial respiration. Compared to MAE, EOMA cells displayed high basal mitochondrial oxygen consumption rate (OCR; **Fig 2a**). NBE treatment alone selectively attenuated basal OCR of EOMA cells. This reduction of OCR was not observed in MAE cells (**Fig. 2a,d**). Elevated basal OCR in EOMA, compared to MAE, was evident even after exposure to weak XRT. Interestingly, weak XRT was observed to offset the effect of NBE in attenuating mitochondrial respiration (**Fig. 2b&d**). Of note, this opposing effect of XRT on NBE was transient and did not hold over time (**Fig. 2b&d**). On the contrary, over time (6-12h), NBE significantly sensitized EOMA, but not MAE, cells to XRT (**Fig. 2c-d**). This observation was consistent with findings on EOMA cell toxicity in response to a combination of NBE and weak XRT (**Fig 1a-b**). MAE cells remained safely unresponsive to such combination treatment (**Fig. 2d**).

Inhibition of tumor cell glycolysis

Extracellular acidification rate (ECAR) is a measure of cellular glycolytic rate (27). EOMA cells displayed 3-fold high basal ECAR than healthy MAE cells (**Fig. 3a,d**). Thus, glycolysis is hyperactive in EOMA cells. NBE successfully compromised the path of glycolytic energy supply specifically in EOMA, but not in MAE, cells at lower dosage of radiation (**Fig. 3a,d**). This effect of NBE, taken together with its inhibitory effect of mitochondrial respiration as addressed above, does achieve substantial functional significance as reflected by the loss of EMOA cell viability (**Fig. 1**). As it relates to the study of healthy MAE, weak XRT accelerated glycolysis (**Fig. 3b-d**). In contrast, weak XRT had no effect on its own on EOMA cells (**Fig. 3b-d**). Interestingly, NBE was effective in inhibition of glycolysis specifically in EOMA cells. Of note, in combination with weak XRT such inhibition of glycolysis was significantly potentiated (**Fig. 3b-d**).

Blunted cellular respiration and reduced ATP production in EOMA cells. Further studies tested the combination of NBE and weak XRT both of which are known to be safe for healthy MAE (**Fig. 1**). The study of cellular bioenergetics showed that both NBE, XRT and their combination had no deleterious effect on MAE cells (**Fig. 4a**). Basal OCR in EOMA cells was 4-fold higher than that in MAE. NBE inhibited OCR in EOMA but not in MAE cells

Antioxidants and Redox Signaling
Mitochondria as Target for Tumor Management of Hemangioendothelioma (DOI: 10.1089/ars.2020.8059)

(**Fig. 4a**). To dissect non-mitochondrial respiration from overall OCR, antimycin A and rotenone were used as inhibitors of complexes III and I, respectively (15). Residual oxygen consumption was 2-fold higher in EOMA compared to MAE cells (**Fig. 4b**). NBE treatment causes significant decrease in the residual oxygen consumption specifically in EOMA cells. Weak XRT alone was more effective than NBE in inhibiting non-mitochondrial respiration. However, a combination of NBE and weak XRT acted co-operatively to specifically inhibit non-mitochondrial respiration of EOMA cells (**Fig. 4b**). Productivity of mitochondrial respiration in EOMA cells was determined by ATP generated through OXPHOS in support of tumor anabolism. EOMA cells demonstrated a 5-fold higher rate of ATP production than that in healthy MAE cells (**Fig. 4c**). Such high rate of ATP production remained unaffected by weak XRT. NBE was potent in blunting the rate of ATP production specifically in EOMA cells. However, in combination with otherwise ineffective weak XRT the effect of NBE was potentiated such that an estimated two-third of the rate of ATP production was inhibited (**Fig. 4c**). Although basal ATP production rate in EOMA was much higher than that of MAE as reported above, total ATP balance in EOMA cells were roughly half of those measured in MAE (**Fig. 4d**). This finding hints towards a very high rate of ATP consumption in EOMA, consistent with its much higher growth rate compared to MAE. NBE, but not weak XRT alone, further depleted ATP levels specifically in EOMA cells. Although ATP levels in EOMA cells were lower than that in MAE cells, the ATP/ADP ratio were comparable. This ratio was markedly decreased in response to NBE. While weak XRT alone did not influence this ratio, together with NBE it further elevated ADP levels in a way that the ratio was further decreased (**Fig. 4e-f**).

Mitochondrial fission and membrane potential. Morphological evidences by electron microscopy shows more abundance of mitochondria in EOMA compared to MAE **(Supplementary Fig. 1)**. NBE induces dynamin-related protein 1 (Drp1), a marker of mitochondrial fission protein, in both MAE as well as EOMA (**Fig 5a,b,c, Supplementary Figs. 2, 3**). Recruitment of Drp1 to mitochondrial tubular network was clearly seen in EOMA cells, however fragmentation was not complete (**Fig S2**). In the presence of weak XRT, such induction was abrogated in MAE but not in EOMA (**Fig 5b,c, Supplementary Fig. 2**). Mitofusin-2 (Mfn-2), a marker of mitochondrial fusion, was more abundant in EOMA

cells compared to MAE (**Fig. 5b,d**). In MAE, not NBE but weak XRT induced Mfn-2. Such weak XRT-dependent induction was blunted in the presence of NBE (**Fig. 5b,d**). Increased expression of mitochondrial fission factor (MFF) and simultaneously decreased dynamin-like protein (OPA1) expression indicate fission in response to combined treatment of NBE and weak XRT (**Fig S4**). Basal mitochondrial copy number in EOMA cells were high compared to MAE (**Fig 5e**). Exposure to NBE reduced the mitochondrial copy number selectively in EOMA but not in MAE (**Fig 5e**). This effect was consistent with exposure to XRT_{weak} and combination of NBE+ XRT_{weak} (**Fig 5e**). In EOMA cells with higher baseline levels of Mfn-2 compared to MAE, NBE lowered the expression of Mfn-2. Interestingly, in these cells, NBE and weak XRT acted co-operatively in markedly lowering the abundance of Mfn-2 (**Fig. 5b,d**). Studies testing additional parameters aimed at rigor showed decreased mitochondrial fusion marker protein (OPA1) and increased mitochondrial fission marker protein (MFF) in response to NBE or NBE+XRT_{weak} combined treatment (**Supplementary Fig. 4**).

Depolarization of the mitochondrial membrane potential (ΔΨm) is a hallmark of compromised mitochondrial function (65). Flow cytometric analyses of mitochondrial ΔΨm revealed that EOMA cells demonstrate 3-fold higher mitochondrial membrane potential under basal conditions compared to that in MAE (**Fig. 5f-i**). In MAE, neither NBE nor weak XRT displayed any effect on mitochondrial membrane potential. However, in EOMA cells, NBE potently compromised mitochondrial membrane potential. Such deleterious effect of NBE on mitochondrial function of EOMA cells was markedly enhanced by the combined treatment of weak XRT (**Fig. 5f-i**). Neither caspase 3 cleavage nor the expression of its upstream regulator caspase 9 were responsive to a combined treatment with NBE and weak XRT (Fig. S3) ruling out the involvement of this particular apoptotic pathway.

Low SIRT3 induces death of EOMA cells. SIRT3 is a mitochondrial protein that contributes to cell survival by a number of mechanisms including regulation of mitochondrial dynamics (3,6,32,43). Abundance of SIRT3 protein was markedly lower in EOMA cells compared to that in MAE (**Fig. 6a**). NBE treatment selectively depleted SIRT3 in EOMA cells, but not that in MAE. In combination with weak XRT, NBE was even more potent in depleting SIRT3 levels in EOMA cells (**Fig. 6b**). To test the functional significance of such SIRT3 depletion in

Antioxidants and Redox Signaling
Mitochondria as Target for Tumor Management of Hemangioendothelioma (DOI: 10.1089/ars.2020.8059)

EOMA cells, pyrroloquinoline quinone (PQQ), a potent inducer of SIRT3, was studied (62). PQQ induced SIRT3 in both cells but the magnitude of induction was much higher in EOMA cells (**Fig. 6c**). The 20 μM dose was chosen for further studies as tangible cytotoxicity was detected with higher dosage (**Fig. 6d**). PQQ treatment restored SIRT3 in EOMA cells treated with a combination of NBE and weak XRT (**Fig. 6f**). Such restoration of SIRT3 abrogated the cytotoxic properties of the combination of NBE and weak XRT (**Fig. 6e**). These findings support the contention that in EOMA cells, SIRT3 depletion causes cell death. Further evidence to rigorously test that contention, a SIRT3 inhibitor LC-0296(1), was utilized. LC-0296 potently depleted SIRT3 in EOMA cells (Fig. 6g). Such severe depletion alone caused EOMA cell death in a way that was more severe than effect of NBE. Taken together, neutralizing SIRT3 is productive in killing EOMA cells. The combination of NBE and weak XRT exploits that avenue of tumor cell death.

AMPK phosphorylation caused by severe depletion of SIRT3 compromises mitochondrial respiration in EOMA cells. Induction of SIRT3 by PQQ lowered phospho-AMPK abundance in both MAE as well as EOMA cells (**Fig. 7a**). Inverse relationship between abundance of SIRT3 and phospho-AMPK was also evident in studies comparing MAE with EOMA. In EOMA, low SIRT3 was associated with high phospho-AMPK (**Fig. 7b-c**). Phospho-AMPK is expressed in a way that is normalized by the overall abundance of AMPK under those conditions. As reported above, NBE treatment compromised mitochondrial function as well as marginally depleted SIRT3 in EOMA cell yet under these conditions phospho-AMPK remained unaffected. However, under conditions of combination treatment with NBE and weak XRT severe depletion of SIRT3 (**Fig. 6a**) elevated phospho-AMPK (**Fig. 7b-c**). PQQ rescued against loss of mitochondrial respiration in EOMA cells treated with a combination of NBE and weak XRT (**Fig. 7d**). Consistently, rescue against loss of membrane potential was also evident in response to PQQ treatment (**Fig. 7e**). These observations argue in favor of a critical role of SIRT3 depletion in causing AMPK phosphorylation followed by mitochondrial dysfunction. Thus, AMPK phosphorylation caused by severe depletion of SIRT3 compromises mitochondrial respiration in EOMA cells.

Improved survival of mice with HE tumor. To determine the functional impact of combination treatment of NBE and weak XRT, mice with hemangioendothelioma (22) in

the control arm received hyaluronic acid cream (29) topically and water orally as vehicle control. The three treatment arms included the following: topical and oral NBE treatment also known as the NBE arm; 7.5 Gy XRT over three days or weak XRT directed at the tumor in 3 fractionated doses; and a combination of the above two also known as the NBE + weak XRT combination treatment group. Tumor volume and blood velocity were determined by Doppler ultrasound (**Fig. 8a**). Tumors in all treatment groups were of the same size on day 3 following EOMA cell injection before beginning any of the therapeutic interventions. In the control arm, rapid increase in tumor volume was noted in 10 days. In this group, the first death was also registered on day 10. Both NBE as well as weak XRT alone significantly limited tumor volume. This effect was most prominent in the combinations treatment group (**Fig. 8b**). As expected, the changes in blood flow velocity showed the same pattern of response as seen with tumor size (**Fig. 8c**). The tumors were also qualitatively different between treatment groups with control animals having large firm slightly spongy blood-filled tumors that had abundant tumor parenchyma and stroma. Irradiated tumors were fluid filled sacs with minimal tumor stroma and no appreciable parenchyma. NBE treated mice had small firm tumors with minimal tumor parenchyma and stroma. NBE and XRT had a fluid filled sac but no appreciable tumor parenchyma or stroma (**Figs. 8d-e**). A Kaplan-Meier survival curve was done in a separate cohort of mice which received the same treatment protocols and results were consistent with the other *in vivo* measurements showing a progressive increase in survival from control, NBE only, weak XRT only, and NBE with XRT (**Fig. 8f**). Thus, both NBE and XRT were able to prolong survival in these mice with the combination of the two treatments being the most effective.

DISCUSSION

DNA damage of tumor cells caused by ionizing radiation has been a productive therapeutic strategy with over two-third of all cancer patients dependent on ionizing radiation therapy (10). This approach targets rapidly proliferating tumor cells justifying its wide usage. However, depending on its dosage, adverse side effects caused by radiation therapy are of serious concern (10). Efforts to find conditions under which low radiation exposure may yield maximum benefits are therefore highly valuable. Radiosensitizers and enhancers are

Antioxidants and Redox Signaling
Mitochondria as Target for Tumor Management of Hemangioendothelioma (DOI: 10.1089/ars.2020.8059)

therefore of interest. To achieve best health outcomes, lower doses of radiation are often used in combination with conventional chemotherapy. While this is of broad interest, this approach has its own limitations primary of which is the fact that in general chemotherapeutic drug themselves are highly cytotoxic not only for tumor cells but also for other healthy cells of the body. The adverse side effects of both radiation as well as chemotherapy pose serious threat to the recovery and quality of life of the surviving patient (9). Phytochemicals, such as anthocyanins, are not only safe but often desirable because of their antioxidant and other beneficial properties (20). An exciting development in tumor management is the observation that dietary phytochemicals exhibit strong chemopreventive properties (33). Our previous work has demonstrated that a standardized natural edible berry extract (NBE) is capable of prolonging survival of mice affected with HE (11). Thus, for certain tumors, these phytochemicals may have a role beyond chemoprevention where therapeutic benefits may be expected. NBE is now awarded FDA IND (**140318**), for human testing against infantile hemangioma. As such efforts progress, it becomes critically important to understand the mechanisms of action of NBE in settings involving vascular neoplasms. Furthermore, it becomes important to ask whether NBE may co-operate with ionizing radiation such that best outcomes may be obtained with radiation so weak that it is otherwise ineffective by itself.

Otto Warburg's proposal of the heavy reliance of cancer cells on aerobic glycolysis, as opposed to mitochondrial OXPHOS, for their energy supply has now evolved to recognize that mitochondrial function is essential for tumor survival. Thus, in addition to applying brakes on the cell cycle, strategies to specifically disrupt mitochondrial function of tumor cells are likely to be valuable (55). A combination approach to target cell cycle as well as mitochondrial function of tumor cells is likely to be productive especially in rapidly growing tumor cells heavily relying on their mitochondrial function for their sustenance. Bioenergetic alterations in tumor cells are diverse. While some are more glycolytic, others rely on OXPHOS of the mitochondria (55). This work presents first evidence on the strikingly hyperactive mitochondria in EOMA cells. In this work, a combination of weak XRT (0.5Gy) and NBE was most effective in killing EOMA cells when only doses that were safe for healthy MAE cells were considered. While NBE alone was effective in causing cell

death, the effect was significantly enhanced by co-treatment with weak XRT. These observations provided the first cues for the design of *in vivo* rescue experiments. Interestingly, mitochondrial oxygen consumption rate of EOMA were three-fold more than that of MAE suggesting heavy reliance of these cells on their mitochondrial function. At dosages used, both NBE as well as weak XRT were safe for MAE. Yet NBE caused marked lowering of mitochondrial respiration. These results are consistent with our earlier findings (4). Weak XRT was also effective in blunting mitochondrial respiration. In combination, NBE and weak XRT severely attenuated mitochondrial function. This work is the first to report on such co-operative effect of a phytochemical and weak XRT on selectively limiting tumor mitochondrial functions in a way that favorably affects tumor outcomes *in vivo*. Glycolysis contributes to tumor cell metabolism. Compared to that of MAE cells, the rate of glycolysis in EOMA was two-fold higher. Specifically, in EOMA cells NBE marginally inhibited glycolysis. Weak XRT induced glycolysis in healthy MAE cells. This observation is consistent with studies testing higher doses of radiation to demonstrate an acute phase of induction of glycolysis (64). In EOMA cells, however, with already high baseline rates of glycolysis, weak XRT inhibited glycolysis in the longer-term. Inhibition of glycolysis in tumor cells by ionizing radiation has been reported (19). High ATP turnover, high proton leak, or elevated non-mitochondrial oxygen consumption may account for high basal respiration of the cell (27). Compared to MAE cells, EOMA cells showed 6-fold higher basal respiration. In the hepatocytes and cardiomyocytes, non-mitochondrial oxygen consumption constitutes approximately 40% of basal OCR, and in endothelial cells approximately 15% (27). In EOMA, non-mitochondrial oxygen consumption accounted for 15% of its basal respiration. Such oxygen consumption is known to contribute to reactive oxygen species (ROS) formation in the cell. EOMA cells, rich in ROS, rely on these oxygen derivatives for their growth (12). NBE inhibited both basal as well as non-mitochondrial respiration of EOMA cells while not affecting MAE cells. While weak XRT had no effect on basal respiration it inhibited non-mitochondrial respiration selectively in EOMA. A combination of NBE and weak XRT did not have any effect on healthy MAE cells. However, it markedly inhibited both basal as well as non-mitochondrial respiration in EOMA cells. While ATP production rate of EOMA cells were 5-fold higher than in MAE cells, ATP balance in these cells was roughly half indicating rapid ATP turnover consistent with its high rate of tumor growth.

Antioxidants and Redox Signaling
Mitochondria as Target for Tumor Management of Hemangioendothelioma (DOI: 10.1089/ars.2020.8059)

ATP/ADP ratio were comparable between MAE and EOMA. NBE lowered the rate of ATP production, depleted ATP content, elevated ADP and lowered ATP/ADP ratio. Such effect was selectively observed in EOMA while MAE cells remained unaffected. While weak XRT did not influence these parameters on its own in either cell type, it potentiated the effect of NBE in lowering the production rate of ATP and elevation of ADP.

Polyphenol-induced loss of tumor mitochondrial function has been recognized as a physicochemical process that cancer cells cannot develop resistance against by gene mutation (39,48). Anthocyanins, rich in berries, are also known to influence mitochondrial dynamics (39). NBE elevated Drp1 in both MAE as well as in EOMA with the distinct contrast that in MAE such increase in fission was not associated with cytotoxicity while in EOMA it was. With respect to the interpretation of significance of such findings it is important to put into context changes in mitochondrial fusion under the same conditions. In MAE, NBE did not influence mitofusin 2. Thus, increased fission in the context of unchanged fusion had no influence on cell viability. In contrast, in EOMA cells, induction of fission was coupled with significant lowering on fusion resulting in loss of cell viability. Thus, unopposed fission killed EOMA cells. Of outstanding interest was the observation that weak XRT did not influence mitochondrial dynamics in both MAE as well as EOMA. However, selectively in EOMA, weak XRT markedly potentiated the inhibitory effect of NBE on fusion. Such synergistic effect is likely to explain the potentiation of EOMA cell death in response to a combination treatment of NBE followed by weak XRT. Fusion of the outer mitochondrial membrane occurs when cells are forced to rely on OXPHOS by withdrawing glucose as a carbon source, thus maximizing OXPHOS by stimulating complementation among mitochondria(35). Impaired fusion and lowered mitochondrial membrane potential favors mitochondrial fragmentation that is often accompanied by bioenergetic defects as has been evident in this work in response to combination treatment(35,49) .SIRT3 has been described as a mitochondria-localized tumor suppressor (30). SIRT3 helps mount mitochondrial adaptive response to stress, such as metabolic reprogramming and antioxidant defense mechanisms. It has thus been recognized that targeting SIRT3 holds promise in tumor management (14). Baseline SIRT3 levels in EOMA cells were observed to be one-third of that observed in non-tumor MAE cells. In EOMA, low SIRT3 was associated

with high phosphorylated AMPK, a key signaling partner of SIRT3 (34). Phosphorylation of AMPK is known to be associated with depleted cellular energy levels as was evident in this work (31). At doses used, both NBE as well as weak XRT did not influence SIRT3 levels in MAE cells. Yet, NBE was effective lowering SIRT3 levels in EOMA from low to deficient. Weak XRT alone had not effect on SIRT3 in EOMA. However, it markedly potentiated the lowering effects of NBE. Plant polyphenols are known to function as natural sirtuin inhibitors (26). Downregulation of SIRT3 is of interest in managing human breast and gastric cancer (17,61). This work presents first evidence that NBE and weak XRT may work synergistically to downregulate SIRT3 in vascular tumor cells. The extraordinary significance of such downregulation with respect to tumor outcomes was highlighted in experiments where the therapeutic effects of such combination therapy was completely abrogated under conditions of pharmacological induction of SIRT3 by PQQ.

Studies on cell biology, as discussed above, lead to the notion that a combination of NBE and weak XRT would be effective in improving health outcomes of hemangioendothelioma. Several previous studies have demonstrated that mice suffering from HE survive roughly for two weeks (11,21). Consistent survival outcomes were observed in this study. Combination therapy with NBE and weak XRT significantly extended lifespan to over six weeks. NBE alone also improved survival. However, weak XRT alone did not. Taken together, this work presents maiden evidence demonstrating the co-operative action of NBE and weak XRT in managing HE. The mechanism of action of this combination therapy includes selective targeting of mitochondrial dynamics and function of tumor cells. Mitochondrial-targeted antitumor therapies are likely to be productive in the management of HE.

MATERIALS AND METHODS

Cell culture. EOMA and murine aortic endothelial (MAE) cells were maintained under the same conditions as previously described (12,23). In brief, cells were maintained in DMEM supplemented with 10% FBS and 1% penicillin/streptomycin (complete media), and incubated at 37^0C and 5% CO2. NBE (200 μg/ml) and vehicle control (1% DMSO) was

Antioxidants and Redox Signaling
Mitochondria as Target for Tumor Management of Hemangioendothelioma (DOI: 10.1089/ars.2020.8059)
This paper has been peer-reviewed and accepted for publication, but has yet to undergo copyediting and proof correction. The final published version may differ from this proof.

carried out in cell culture media for 24 hours prior to initiating experiments. NBE is a proprietary mix of powdered berry extracts (PediaBerry™, NutrimiR, Columbus, OH).

Extracellular flux and oxygen consumption rate (Seahorse™) assays. Oxygen Consumption Rate (OCR) and Extracellular Acidification Rate (ECAR) measurements were performed using a Seahorse Bioscience XF-96 instrument as described previously (16,45). In brief, a day prior to the experiment, the sensor cartridge was hydrated overnight using the calibration buffer supplied by the manufacturer (Seahorse Biosciences, Santa Clara, CA, USA). The NBE treated cells were seeded in the 96 well microplate in complete DMEM media with 4.5g/L of glucose. On the day of the experiment, the cells were washed with calibration buffer twice and incubated with glucose free Seahorse XF base medium supplemented with 25mM of glucose for 1h at 37°C in a CO2 free incubator. The injection ports of the sensors were filled with 20 µL of treatment or vehicle in buffer. The sensor was then placed into the XF-96 instrument and calibrated. After calibration, the calibration fluid plate was replaced with the cell plate. The measurement cycle consisted of a 2 min mix, 1 min wait, and a 2 min measurement. Four basal rate measurements were followed by sequential addition of oligomycin (8µg/ml), carbonylcyanide-3-chlorophenylhydrazone (CCCP, 100µM), rotenone (100µM), and antimycin A (100µM) prepared in glucose free Seahorse XF base medium. Each injection was followed by four measurement cycles. The consumption rates were calculated from the continuous average slope of the decreased O2 using a compartmentalization model(36) . For any one treatment, the rates from 10 wells were used. Rates for the wells were normalized for protein content.

Determination of cell viability. Cell viability was measured by leakage of lactate dehydrogenase (LDH) from cells to media using the in vitro toxicology assay kit from Sigma Chemical (St Louis, MO, USA) as described (12). Cell viability was also analyzed by propidium iodide (PI) exclusion test. Cells were incubated with PI (2.5 mmol/L) in phosphate-buffered saline for 15 minutes at 37°C and with 5%CO_2. Fluorescence intensity was determined by FACS using PI staining in the FL2 region using an Accuri C6 Flow Cytometer (Accuri, Ann Arbor, MI) at 530-nm excitation with a gated sample size of 10,000 cells (12,41).

Antioxidants and Redox Signaling
Mitochondria as Target for Tumor Management of Hemangioendothelioma (DOI: 10.1089/ars.2020.8059)

Measurement of mitochondrial membrane potential. Mitochondrial membrane potential changes were analyzed using the lipophilic cationic dye JC-1 (MitoProbe JC-1 Assay Kit for Flow Cytometry, Life technologies) per manufacturer's instruction by flow cytometer as reported previously (8).

Determination of ADP/ATP levels. Changes in the ADP/ATP ratio were measured using bioluminescent assay (EnzyLightTM ADP/ATP Ratio Assay Kit; BioAssay Systems) as described previously (42). The ATP content in each sample was corrected for the protein concentration that was determined with the bicinchoninic acid (BCA) protein assay (Pierce).

Western blot. Immunoblotting was performed using cell lysates and the protein concentration determined using a BCA protein assay. Samples (15-20 µg of protein / lane) were separated using 4-12% SDS polyacrylamide gel electrophoresis and probed with Rabbit monoclonal anti-Mitofusin 2 antibody (1:1000 dilution, Cat no # ab124773, Abcam, Cambridge, MA), rabbit monoclonal anti-Drp1 antibody (1:1000 dilution, Cat no # ab184247, Abcam, Cambridge, MA), anti-OPA1 antibody (1:1000 dilution, Cat no # 1284B, Novus Biologicals, Centennial, CO), Anti-MFF antibody (1:500 dilution, Cat no # ab129075, Abcam, Cambridge, MA) anti-phos-AMPK (1:1000 dilution, Cat no # PA5-17831, ThermoFisher Scientific, Grand Island, NY), anti-AMPK (1:1000 dilution, Cat no # NB100-239, Novus Biologicals, Littleton, CO), rabbit polyclonal anti-SIRT3 antibody (1:100 dilution, Cat no # ab86671, Abcam, Cambridge, MA) and anti-mouse ß-actin (1:10000 dilution, Cat no # A5441, Lot. #055K4854 Sigma, St. Louis, MO). Bands were visualized by using horseradish peroxidase conjugated donkey anti-rabbit-IgG (1:2000, Cat no # NA934V, Lot # 9583369, Amersham Biosciences, Piscataway, NJ) and anti-mouse-IgG (1:2000, Cat no # NA931V, Lot # 6652622, Amersham Biosciences, Piscataway, NJ) (11,12,24) and the enhanced chemiluminescence assay (Amersham Biosciences, Piscataway, NJ) according to the manufacturer's instructions. Pixel densitometry for individual bands was done using image J software.

SIRT3 ELISA. Cells were seeded in 12-well plates at 0.1 X 10^6 cells/well. SIRT3 ELISA was performed on cell pellets by using the SIRT 3 ELISA kit (Cal no # MBS2023250, MY

Biosciences, San Diego, CA) according to the manufacturer's instructions. BCA protein assay was performed on an aliquot of all tested samples and the results standardized per milligram of protein.

Transmission Electron Microscopy (TEM). TEM was done as per our previous report(57). Briefly, primary fixation of the cells was done with 3% Glutaraldehyde in 0.1M phosphate buffer. After rinsing in buffer, post fixation followed for 1 hour with 1% osmium tetroxide in 0.1M phosphate buffer. After dehydration using ethyl alcohol and acetone as an intermediate solvent, cells were infiltrated over the weekend in ½ acetone and ½ embedding media. They were then embedded in fresh resin (Embed 812, Electron Microscopy Sciences, Hatfield, PA). Following polymerization overnight at 60°C the blocks were then ready to section. All steps were done in small centrifuge tubes, including embedding. Thin sections were cut (80-90nm), stained with UA replacement stain, (Electron Microscopy Sciences, Hatfield, PA) then viewed on a Tecnai Spirit (ThermoFisher, Hillsboro, OR). Digital images were taken with an AMT (Advanced Microscopy Techniques, Danvers, MA) CCD camera.

Ultrasound imaging. A high-frequency, high-resolution ultrasound imaging system (Vevo 2100; Visual-Sonics, Toronto, Canada) with a MS 550D (22-55 MHz) linear array transducer was used as described previously(18,45,46). Mice were anesthetized using a mixture of 1.5% isoflurane inhalant anesthesia with 95% oxygen and animals were placed in the supine position on a moveable, heated stage maintained at 37°C. Hair was removed from tumors using a depilatory cream. Ultrasound scan transmission gel was applied to the tumor surface and the probe was positioned on a fixed stand perpendicular to the stage. The image resolution was maintained at 100 µm laterally and 50 µm axially. B-mode mapping was performed until clearly visualized the tumor anatomical location. Each targeted tumor was visualized in two-dimensional (2D) imaging for the visualization of the tumor. Fine position adjustment was done for the highest signal intensity with continuous adjustment of contrast, dynamic range, and gain until the minimal noise appeared in the background. For tumor volume measurement, different location on the tumor was setup with the transducer and B-mode recordings were made with the ultrasound beam perpendicular to the targeted tumor. Several recordings (cine-loops), each up to 5

Antioxidants and Redox Signaling
Mitochondria as Target for Tumor Management of Hemangioendothelioma (DOI: 10.1089/ars.2020.8059)

seconds, of B-mode were saved. Color Doppler flowmetry of tumor vasculature and tumor feeder vessel flow were also recorded using color Doppler flow imaging (CFI) mode in 2D mode.

The tumor volume was measured during post-processing. VevoLab software (Visual Sonics) was used to compile each 2D image slice with other acquired slices and traced the area and depth of the wound resulting into a volumetric data. From the real-time B-mode observation, the frame-wise tracing of tumor edge borders were performed.

***In vitro* XRT**. Cells were pretreated with NBE (200µg/ml) or vehicle (1% DMSO) for 24h. For the XRT exposure experiments, one multi-well plate was used as an unexposed control and other plates were exposed to either 0.5 (weak) or 1Gy of XRT using an XRT unit (Precision, north Branford, CT) (28,54). 6 or 12h after exposure with XRT, cells were collected for further analysis. Here NBE treated non-irradiated cells were maintained with the exact time points matched with NBE exposure of irradiated cells.

***In vivo* weak XRT**. All animal protocols were approved by the Institutional Animal Care and Use Committee (IACUC) of the Ohio State University, Columbus, Ohio. Mice were maintained under standard conditions at 22+2°C with 12:12 dark: light cycles with access to food and water ad libitum. 129P/3 mice (6-8 weeks, female, Jackson Laboratories, Bar Harbor, ME Indianapolis, IN) were subcutaneously injected with vehicle, EOMA cells, as previously described (12). Mice were treated with oral gavaging of NBE (20mg/kg) and topical application (200mg/kg) once daily (11). Mice were radiated with 2.5Gy gamma XRT per dose directed at the tumor given on the 3rd, 5th and 7th day after EOMA cell injection for a total dose of 7.5 Gy. On the 10th day after cell injections mice were sacrificed and tumor volume was determined by using calipers to measure length × width × height of each tumor as previously described (11,21).

Immunocytochemistry (ICC) and confocal microscopy. For immunocytochemistry, cells (50,000 cells/well) were seeded on a coverslip. Cells were exposed to treatment after adhering to the cover slips. Post treatment, all experimental groups were incubated in DMEM (4.5g/l glucose) containing 250nM MitoTracker™ Red CMXRos at 37° C for 30 minutes. After staining with MitoTracker™ Red CMXRos, the cover slips were washed once

in PBS and fixed with 4% paraformaldehyde solution made in PBS prior to blocking with 10% NGS. Cells were then incubated with Anti-Drp1 (1:50 dilution, Cat no # ab184247) at 4°C overnight. Signal was visualized by subsequent incubation with fluorescence-tagged appropriate secondary antibodies. Fluorescent stained slides were counter stained with DAPI. Confocal microscopy was performed using a ZEISS LSM 880 (Germany). Co-localization was quantified using co-localization plug-in of Zeiss software (Zen, blue edition) as per our previous reports(45-47). Pearson correlation coefficient was determined for each cell as a measure of co-localization and was expressed as means ± S.D.

mtDNA copy number determination. Extracted DNAs (DNeasy Blood & Tissue Kit, QIAGEN, Germantown, MD) from EOMA and MAE cells exposed to different conditions were used to measure mitochondrial to nuclear DNA ratio using PCR format per manufacturer's instructions (NovaQUANT™ Mouse Mitochondrial to Nuclear Ratio kit, EMD Millipore, Billerica, MA). Data was presented as mtDNA copy numbers as described previously(2).

Mitochondrial mass determination. It was done using MitoTracker® green FM. After treating with NBE or vehicle for 24 hours, cell pellet was obtained by centrifugation. Cells were resuspended in prewarmed DMEM media containing 25nM of MitoTracker® green FM (Invitrogen M7514) and incubated for 30 minutes at 37°C. After incubation, cells were washed two times with PBS and resuspended again in fresh medium and analyzed by flow cytometry to access the mitochondrial mass.

Statistical methods. Two-sided two-sample t tests were used to compare the differences between two groups with proper data transformation. Residual data from every test were investigated to ensure that the normality assumptions of the model were satisfied. Sensitivity analyses were also conducted using nonparametric procedures to ensure that the conclusions were robust to the selection of the statistical methods. The statistician was completely blinded about the study. A Kaplan-Meier survival analysis with log rank test was to compare different groups. A sample size of 5 for each group will provide at least 80% power of detecting a 2-fold change of each miRNA at type I error α=0.01 and assuming a 25% Coefficient of Variation (CV) based on a two sided two sample t-test for cell or in vitro experiment. Replication of 5 in each treatment group provided 80% power

to identify the best dose that is approximately 1.0 standard deviation better than the next best dose at $\alpha = 0.05$. A one-side log rank test with sample size of 5 per group provide 80% power at significance level of 0,05 to detect proportion of survival of 20% for control and 80% for combined treatment at day 14. A p value of <0.05 was considered statistically significant for each experiment.

Conflict of interest

The standardized Natural Berry Extract has been commercialized via a university startup company in which CKS is a shareholder.

Author contributions

Conceptualization, A.B., G.G., K.S. and C.K.S; Methodology, A.B., G.G., K.S., S.K, P.G., and C.K.S; Investigation and Validation, A.B., A.S., P.G., C.M. and K.S.; Formal Analysis, A.B., X.F.; KS; Writing, CKS (final); Original Draft, A.B., G.G.; K.S., E.C., S.K., and C.K.S; Funding Acquisition, G.G and C.K.S.; Resources, G.G and C.K.S.; Supervision, G.G., S.K, and C.K.S.

Acknowledgment

We thank Ohio State University Laboratory Animal Resources for care of mice in accordance with National Institutes of Health (NIH) guidelines. We thank Joseph Dynlacht and Joy Garrett, Radiation Oncology, IUSM for their help in in vitro radiation experiments. This study was supported by GM095657 to GG and in part by NIH RO1 grants GM069589, GM077185, GM108014 and NR013898 to CKS.

REFERENCES

1. Alhazzazi TY, Kamarajan P, Xu Y, Ai T, Chen L, Verdin E, Kapila YL. A Novel Sirtuin-3 Inhibitor, LC-0296, Inhibits Cell Survival and Proliferation, and Promotes Apoptosis of Head and Neck Cancer Cells. *Anticancer Res* 36: 49-60, 2016.
2. Aminzadeh MA, Rogers RG, Fournier M, Tobin RE, Guan X, Childers MK, Andres AM, Taylor DJ, Ibrahim A, Ding X, Torrente A, Goldhaber JM, Lewis M, Gottlieb RA, Victor RA, Marban E. Exosome-Mediated Benefits of Cell Therapy in Mouse and Human Models of Duchenne Muscular Dystrophy. *Stem Cell Reports* 10: 942-955, 2018.
3. Ansari A, Rahman MS, Saha SK, Saikot FK, Deep A, Kim KH. Function of the SIRT3 mitochondrial deacetylase in cellular physiology, cancer, and neurodegenerative disease. *Aging Cell* 16: 4-16, 2017.
4. Atalay M, Gordillo G, Roy S, Rovin B, Bagchi D, Bagchi M, Sen CK. Anti-angiogenic property of edible berry in a model of hemangioma. *FEBS Lett* 544: 252-7, 2003.
5. Aune D, Giovannucci E, Boffetta P, Fadnes LT, Keum N, Norat T, Greenwood DC, Riboli E, Vatten LJ, Tonstad S. Fruit and vegetable intake and the risk of cardiovascular disease, total cancer and all-cause mortality-a systematic review and dose-response meta-analysis of prospective studies. *Int J Epidemiol* 46: 1029-1056, 2017.
6. Bagul PK, Katare PB, Bugga P, Dinda AK, Banerjee SK. SIRT-3 Modulation by Resveratrol Improves Mitochondrial Oxidative Phosphorylation in Diabetic Heart through Deacetylation of TFAM. *Cells* 7, 2018.
7. Bajzikova M, Kovarova J, Coelho AR, Boukalova S, Oh S, Rohlenova K, Svec D, Hubackova S, Endaya B, Judasova K, Bezawork-Geleta A, Kluckova K, Chatre L, Zobalova R, Novakova A, Vanova K, Ezrova Z, Maghzal GJ, Magalhaes Novais S, Olsinova M, Krobova L, An YJ, Davidova E, Nahacka Z, Sobol M, Cunha-Oliveira T, Sandoval-Acuña C, Strnad H, Zhang T, Huynh T, Serafim TL, Hozak P, Sardao VA, Koopman WJH, Ricchetti M, Oliveira PJ, Kolar F, Kubista M, Truksa J, Dvorakova-Hortova K, Pacak K, Gurlich R, Stocker R, Zhou Y, Berridge MV, Park S, Dong L, Rohlena J, Neuzil J. Reactivation of Dihydroorotate Dehydrogenase-Driven Pyrimidine Biosynthesis Restores Tumor Growth of Respiration-Deficient Cancer Cells. *Cell Metab* 29: 399-416.e10, 2019.

8. Banerjee J, Das Ghatak P, Roy S, Khanna S, Sequin EK, Bellman K, Dickinson BC, Suri P, Subramaniam VV, Chang CJ, Sen CK. Improvement of human keratinocyte migration by a redox active bioelectric dressing. *PLoS One* 9: e89239, 2014.

9. Baskar R, Itahana K. Radiation therapy and cancer control in developing countries: Can we save more lives? *Int J Med Sci* 14: 13-17, 2017.

10. Berkey FJ. Managing the adverse effects of radiation therapy. *Am Fam Physician* 82: 381-8, 394, 2010.

11. Biswas A, Clark EC, Sen CK, Gordillo GM. Phytochemical Inhibition of Multidrug Resistance Protein-1 as a Therapeutic Strategy for Hemangioendothelioma. *Antioxid Redox Signal* 26: 1009-1019, 2017.

12. Biswas A, Khanna S, Roy S, Pan X, Sen CK, Gordillo GM. Endothelial cell tumor growth is Ape/ref-1 dependent. *Am J Physiol Cell Physiol* 309: C296-307, 2015.

13. Cavalli LR, Varella-Garcia M, Liang BC. Diminished tumorigenic phenotype after depletion of mitochondrial DNA. *Cell Growth Differ* 8: 1189-98, 1997.

14. Chen Y, Fu LL, Wen X, Wang XY, Liu J, Cheng Y, Huang J. Sirtuin-3 (SIRT3), a therapeutic target with oncogenic and tumor-suppressive function in cancer. *Cell Death Dis* 5: e1047, 2014.

15. Cummings BS, Schnellmann RG. Measurement of cell death in mammalian cells. *Curr Protoc Pharmacol* Chapter 12: Unit 12 8, 2004.

16. Deng B, Ghatak S, Sarkar S, Singh K, Das Ghatak P, Mathew-Steiner SS, Roy S, Khanna S, Wozniak DJ, McComb DW, Sen CK. Novel Bacterial Diversity and Fragmented eDNA Identified in Hyperbiofilm-Forming Pseudomonas aeruginosa Rugose Small Colony Variant. *iScience* 23: 100827, 2020.

17. Finley LW, Carracedo A, Lee J, Souza A, Egia A, Zhang J, Teruya-Feldstein J, Moreira PI, Cardoso SM, Clish CB, Pandolfi PP, Haigis MC. SIRT3 opposes reprogramming of cancer cell metabolism through HIF1alpha destabilization. *Cancer Cell* 19: 416-28, 2011.

18. Gallego-Perez D, Pal D, Ghatak S, Malkoc V, Higuita-Castro N, Gnyawali S, Chang L, Liao WC, Shi J, Sinha M, Singh K, Steen E, Sunyecz A, Stewart R, Moore J, Ziebro T, Northcutt RG, Homsy M, Bertani P, Lu W, Roy S, Khanna S, Rink C, Sundaresan VB, Otero JJ, Lee LJ, Sen CK. Topical tissue nano-transfection mediates non-viral stroma reprogramming and rescue. *Nat Nanotechnol* 12: 974-979, 2017.

19. Ganapathy-Kanniappan S, Geschwind JF. Tumor glycolysis as a target for cancer therapy: progress and prospects. *Mol Cancer* 12: 152, 2013.

20. Gomez de Cedron M, Vargas T, Madrona A, Jimenez A, Perez-Perez MJ, Quintela JC, Reglero G, San-Felix A, Ramirez de Molina A. Novel Polyphenols That Inhibit Colon Cancer Cell Growth Affecting Cancer Cell Metabolism. *J Pharmacol Exp Ther* 366: 377-389, 2018.

21. Gordillo G, Fang H, Khanna S, Harper J, Phillips G, Sen CK. Oral administration of blueberry inhibits angiogenic tumor growth and enhances survival of mice with endothelial cell neoplasm. *Antioxid Redox Signal* 11: 47-58, 2009.

22. Gordillo GM, Atalay M, Roy S, Sen CK. Hemangioma model for in vivo angiogenesis: inducible oxidative stress and MCP-1 expression in EOMA cells. *Methods Enzymol* 352: 422-32, 2002.

23. Gordillo GM, Biswas A, Khanna S, Pan X, Sinha M, Roy S, Sen CK. Dicer knockdown inhibits endothelial cell tumor growth via microRNA 21a-3p targeting of Nox-4. *J Biol Chem* 289: 9027-38, 2014.

24. Gordillo GM, Biswas A, Khanna S, Spieldenner JM, Pan X, Sen CK. Multidrug Resistance-associated Protein-1 (MRP-1)-dependent Glutathione Disulfide (GSSG) Efflux as a Critical Survival Factor for Oxidant-enriched Tumorigenic Endothelial Cells. *J Biol Chem* 291: 10089-103, 2016.

25. Hayashi J, Takemitsu M, Nonaka I. Recovery of the missing tumorigenicity in mitochondrial DNA-less HeLa cells by introduction of mitochondrial DNA from normal human cells. *Somat Cell Mol Genet* 18: 123-9, 1992.

26. Heger V, Tyni J, Hunyadi A, Horakova L, Lahtela-Kakkonen M, Rahnasto-Rilla M. Quercetin based derivatives as sirtuin inhibitors. *Biomed Pharmacother* 111: 1326-1333, 2019.

27. Hill BG, Benavides GA, Lancaster JR, Jr., Ballinger S, Dell'Italia L, Jianhua Z, Darley-Usmar VM. Integration of cellular bioenergetics with mitochondrial quality control and autophagy. *Biol Chem* 393: 1485-1512, 2012.

28. Jaillet C, Morelle W, Slomianny MC, Paget V, Tarlet G, Buard V, Selbonne S, Caffin F, Rannou E, Martinez P, Francois A, Foulquier F, Allain F, Milliat F, Guipaud O. Radiation-induced changes in the glycome of endothelial cells with functional consequences. *Sci Rep* 7: 5290, 2017.

29. Jegasothy SM, Zabolotniaia V, Bielfeldt S. Efficacy of a New Topical Nano-hyaluronic Acid in Humans. *J Clin Aesthet Dermatol* 7: 27-9, 2014.

30. Kim HS, Patel K, Muldoon-Jacobs K, Bisht KS, Aykin-Burns N, Pennington JD, van der Meer R, Nguyen P, Savage J, Owens KM, Vassilopoulos A, Ozden O, Park SH, Singh KK, Abdulkadir SA, Spitz DR, Deng CX, Gius D. SIRT3 is a mitochondria-localized tumor suppressor required for maintenance of mitochondrial integrity and metabolism during stress. *Cancer Cell* 17: 41-52, 2010.

31. Kim J, Yang G, Kim Y, Kim J, Ha J. AMPK activators: mechanisms of action and physiological activities. *Exp Mol Med* 48: e224, 2016.

32. Klimova N, Long A, Kristian T. Nicotinamide mononucleotide alters mitochondrial dynamics by SIRT3-dependent mechanism in male mice. *J Neurosci Res* 97: 975-990, 2019.

33. Kotecha R, Takami A, Espinoza JL. Dietary phytochemicals and cancer chemoprevention: a review of the clinical evidence. *Oncotarget* 7: 52517-52529, 2016.

34. Li S, Dou X, Ning H, Song Q, Wei W, Zhang X, Shen C, Li J, Sun C, Song Z. Sirtuin 3 acts as a negative regulator of autophagy dictating hepatocyte susceptibility to lipotoxicity. *Hepatology* 66: 936-952, 2017.

35. Maycotte P, Marín-Hernández A, Goyri-Aguirre M, Anaya-Ruiz M, Reyes-Leyva J, Cortés-Hernández P. Mitochondrial dynamics and cancer. *Tumour Biol* 39: 1010428317698391, 2017.

36. Mookerjee SA, Gerencser AA, Nicholls DG, Brand MD. Quantifying intracellular rates of glycolytic and oxidative ATP production and consumption using extracellular flux measurements. *J Biol Chem* 292: 7189-7207, 2017.

37. Morais R, Zinkewich-Peotti K, Parent M, Wang H, Babai F, Zollinger M. Tumor-forming ability in athymic nude mice of human cell lines devoid of mitochondrial DNA. *Cancer Res* 54: 3889-96, 1994.

38. Nayler SJ, Rubin BP, Calonje E, Chan JK, Fletcher CD. Composite hemangioendothelioma: a complex, low-grade vascular lesion mimicking angiosarcoma. *Am J Surg Pathol* 24: 352-61, 2000.

39. Parrado-Fernandez C, Sandebring-Matton A, Rodriguez-Rodriguez P, Aarsland D, Cedazo-Minguez A. Anthocyanins protect from complex I inhibition and APPswe mutation through modulation of the mitochondrial fission/fusion pathways. *Biochim Biophys Acta* 1862: 2110-2118, 2016.

40. Prencipe FP, Bruni R, Guerrini A, Rossi D, Benvenuti S, Pellati F. Metabolite profiling of polyphenols in Vaccinium berries and determination of their chemopreventive properties. *J Pharm Biomed Anal* 89: 257-67, 2014.

41. Riccardi C, Nicoletti I. Analysis of apoptosis by propidium iodide staining and flow cytometry. *Nat Protoc* 1: 1458-61, 2006.

42. Rink C, Gnyawali S, Peterson L, Khanna S. Oxygen-inducible glutamate oxaloacetate transaminase as protective switch transforming neurotoxic glutamate to metabolic fuel during acute ischemic stroke. *Antioxid Redox Signal* 14: 1777-85, 2011.

43. Samant SA, Zhang HJ, Hong Z, Pillai VB, Sundaresan NR, Wolfgeher D, Archer SL, Chan DC, Gupta MP. SIRT3 deacetylates and activates OPA1 to regulate mitochondrial dynamics during stress. *Mol Cell Biol* 34: 807-19, 2014.

44. Shimura T, Sasatani M, Kawai H, Kamiya K, Kobayashi J, Komatsu K, Kunugita N. A comparison of radiation-induced mitochondrial damage between neural progenitor stem cells and differentiated cells. *Cell Cycle* 16: 565-573, 2017.

45. Singh K, Pal D, Sinha M, Ghatak S, Gnyawali SC, Khanna S, Roy S, Sen CK. Epigenetic Modification of MicroRNA-200b Contributes to Diabetic Vasculopathy. *Mol Ther* 25: 2689-2704, 2017.

46. Singh K, Sinha M, Pal D, Tabasum S, Gnyawali SC, Khona D, Sarkar S, Mohanty SK, Soto-Gonzalez F, Khanna S, Roy S, Sen CK. Cutaneous Epithelial to Mesenchymal Transition Activator ZEB1 Regulates Wound Angiogenesis and Closure in a Glycemic Status Dependent Manner. *Diabetes*, 2019.

47. Sinha M, Sen CK, Singh K, Das A, Ghatak S, Rhea B, Blackstone B, Powell HM, Khanna S, Roy S. Direct conversion of injury-site myeloid cells to fibroblast-like cells of granulation tissue. *Nat Commun* 9: 936, 2018.

48. Stevens JF, Revel JS, Maier CS. Mitochondria-Centric Review of Polyphenol Bioactivity in Cancer Models. *Antioxid Redox Signal* 29: 1589-1611, 2018.

49. Suárez-Rivero JM, Villanueva-Paz M, de la Cruz-Ojeda P, de la Mata M, Cotán D, Oropesa-Ávila M, de Lavera I, Álvarez-Córdoba M, Luzón-Hidalgo R, Sánchez-Alcázar JA. Mitochondrial Dynamics in Mitochondrial Diseases. *Diseases* 5, 2016.

50. Sullivan LB, Gui DY, Hosios AM, Bush LN, Freinkman E, Vander Heiden MG. Supporting Aspartate Biosynthesis Is an Essential Function of Respiration in Proliferating Cells. *Cell* 162: 552-63, 2015.

51. Sullivan LB, Gui DY, Vander Heiden MG. Altered metabolite levels in cancer: implications for tumour biology and cancer therapy. *Nat Rev Cancer* 16: 680-693, 2016.

52. Thomasset SC, Berry DP, Garcea G, Marczylo T, Steward WP, Gescher AJ. Dietary polyphenolic phytochemicals--promising cancer chemopreventive agents in humans? A review of their clinical properties. *Int J Cancer* 120: 451-8, 2007.

53. Viale A, Corti D, Draetta GF. Tumors and mitochondrial respiration: a neglected connection. *Cancer Res* 75: 3685-6, 2015.

54. Vieira Dias J, Gloaguen C, Kereselidze D, Manens L, Tack K, Ebrahimian TG. Gamma Low-Dose-Rate Ionizing Radiation Stimulates Adaptive Functional and Molecular Response in Human Aortic Endothelial Cells in a Threshold-, Dose-, and Dose Rate-Dependent Manner. *Dose Response* 16: 1559325818755238, 2018.

55. Wallace DC. Mitochondria and cancer. *Nat Rev Cancer* 12: 685-98, 2012.

56. Wang LS, Stoner GD. Anthocyanins and their role in cancer prevention. *Cancer Lett* 269: 281-90, 2008.

57. Wang M, Smith K, Yu Q, Miller C, Singh K, Sen CK. Mitochondrial connexin 43 in sex-dependent myocardial responses and estrogen-mediated cardiac protection following acute ischemia/reperfusion injury. *Basic Res Cardiol* 115: 1, 2019.

58. Wang X, Ouyang Y, Liu J, Zhu M, Zhao G, Bao W, Hu FB. Fruit and vegetable consumption and mortality from all causes, cardiovascular disease, and cancer: systematic review and dose-response meta-analysis of prospective cohort studies. *BMJ* 349: g4490, 2014.

59. Weiss SW, Enzinger FM. Epithelioid hemangioendothelioma: a vascular tumor often mistaken for a carcinoma. *Cancer* 50: 970-81, 1982.

60. Wen YA, Xiong X, Scott T, Li AT, Wang C, Weiss HL, Tan L, Bradford E, Fan TWM, Chandel NS, Barrett TA, Gao T. The mitochondrial retrograde signaling regulates Wnt signaling to promote tumorigenesis in colon cancer. *Cell Death Differ* 26: 1955-1969, 2019.

61. Yang B, Fu X, Shao L, Ding Y, Zeng D. Aberrant expression of SIRT3 is conversely correlated with the progression and prognosis of human gastric cancer. *Biochem Biophys Res Commun* 443: 156-60, 2014.

62. Zhang J, Meruvu S, Bedi YS, Chau J, Arguelles A, Rucker R, Choudhury M. Pyrroloquinoline quinone increases the expression and activity of Sirt1 and -3 genes in HepG2 cells. *Nutr Res* 35: 844-9, 2015.

63. Zhang J, Wu B, Zhou GQ, Zhang RS, Wei X, Yu B, Lu ZF, Ma HH, Shi QL, Zhou XJ. Composite hemangioendothelioma arising from the kidney: case report with review of the literature. *Int J Clin Exp Pathol* 6: 1935-41, 2013.

64. Zhong J, Rajaram N, Brizel DM, Frees AE, Ramanujam N, Batinic-Haberle I, Dewhirst MW. Radiation induces aerobic glycolysis through reactive oxygen species. *Radiother Oncol* 106: 390-6, 2013.

65. Zorova LD, Popkov VA, Plotnikov EY, Silachev DN, Pevzner IB, Jankauskas SS, Babenko VA, Zorov SD, Balakireva AV, Juhaszova M, Sollott SJ, Zorov DB. Mitochondrial membrane potential. *Anal Biochem* 552: 50-59, 2018.

Figure Legends

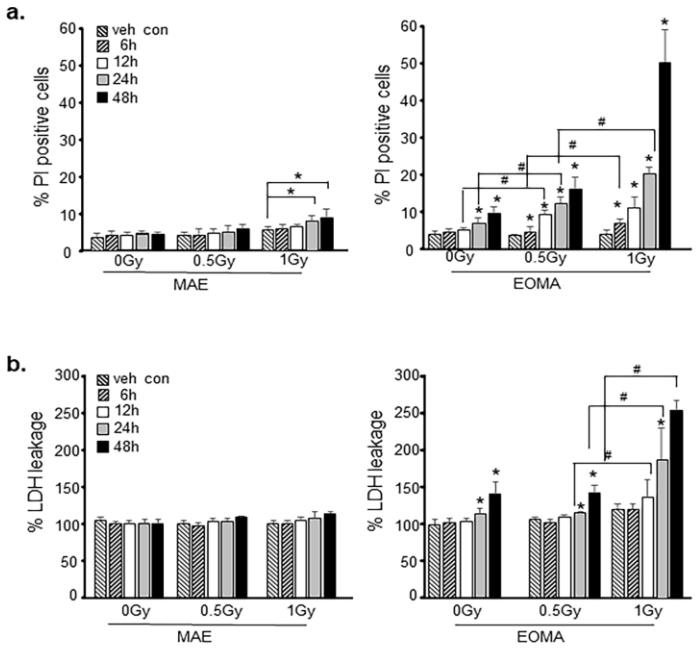

Fig. 1

FIGURE 1

Sensitization of tumor forming endothelial cells to effects of XRT is time and dose dependent.

a, EOMA and MAE cells were treated with NBE (200µg/ml) and vehicle (1% DMSO) for 6, 12, 24 and 48h. In some treatment group, 0.5 and 1Gy of X-ray radiation was exposed for 6h after NBE treatment schedule. Cell viability was measured by flow cytometry using PI (10µg/ml) exclusion and (**b**) LDH toxicity assay (Sigma-Aldrich, MAK066) shows a dose dependent decrease in EOMA cell survival. MAE cells were included as non-tumor forming endothelial cell controls. The key indicates the time of sample collection after XRT or after the 24-hour pre-treatment period for those samples that were not irradiated. *p <0.05, n=6.

Antioxidants and Redox Signaling
Mitochondria as Target for Tumor Management of Hemangioendothelioma (DOI: 10.1089/ars.2020.8059)

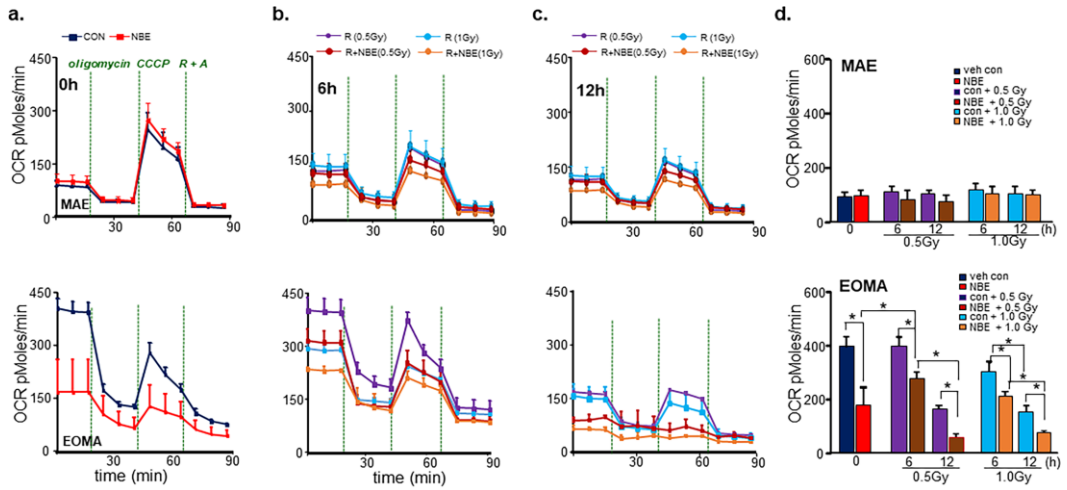

Fig. 2

FIGURE 2

NBE sensitized EOMA, not MAE, cells to weak XRT by inhibiting mitochondrial respiration.

NBE/vehicle treated MAE, EOMA cells were seeded (5000cells/well) in a Seahorse XF 96 well plate. After the indicated time points of treatment schedule Oxygen consumption rate (OCR) was determined during sequential treatments with oligomycin (ATP-synthase inhibitor; 8mg/ml), CCCP a protonophore that lowers the mitochondrial membrane potential to create conditions for maximal oxidative respiration (100mM), and antimycin-A (100mM) + rotenone (100mM) to inhibit the electron transport chain. **a**, Vehicle controls were treated with 1% DMSO. Cells were exposed to XRT alone (0.5/1.0 Gy) or in combination of NBE and XRT for 6h (**b**) and 12h (**c**) exposure as mentioned earlier. **d**, bar graph comparing basal OCR under all treatment conditions shows decreased OCR after weak XRT exposure in NBE treated EOMA cells. But there was no such observation was found in case of MAE cells. Results were expressed as means ± SD (n=6).

Antioxidants and Redox Signaling
Mitochondria as Target for Tumor Management of Hemangioendothelioma (DOI: 10.1089/ars.2020.8059)

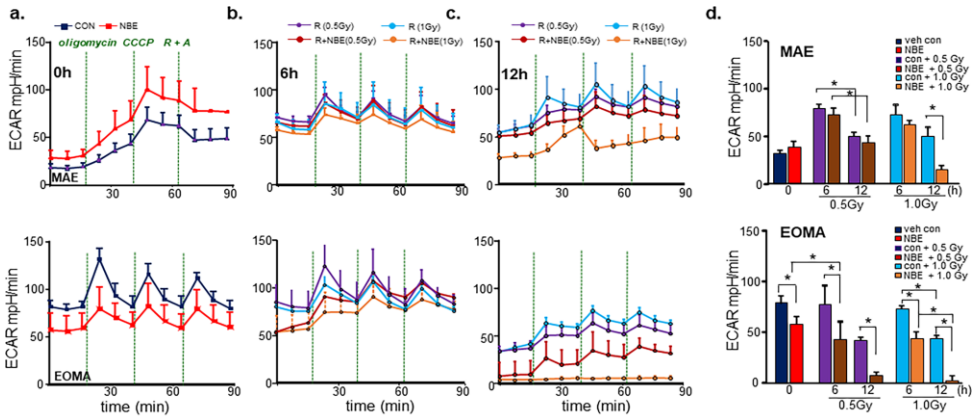

Fig. 3

FIGURE 3

Inhibition of tumor cell glycolysis by NBE alone, and more so in combination with weak XRT.

NBE/vehicle treated MAE, EOMA cells were seeded (5000cells/well) in a Seahorse XF 96 well plate. After the indicated time points of treatment schedule extracellular acidification rate (ECAR) of cells was determined by Seahorse XF96 analyzer, upon sequential addition of oligomycin (100mM), CCCP (100mM), and antimycin-A (100mM) + rotenone (100mM). One of 3 experiments is shown as representation. **a**, Only NBE exposure significantly inhibits ECAR levels in EOMA cells not in MAE. **b**, Representative bar graph shows ECAR levels was further inhibited with the exposure of either weak XRT or XRT at 6h which was not observed in MAE cells but with longer exposure (12h), MAE cells shows significant reduction in ECAR level (**c**). The representative bar graph shows decreased ECAR after weak XRT/XRT exposure in NBE treated EOMA cells. But there was only with NBE with XRT exposure in MAE cell causes inhibition of ECAR activity. Thus 0.5Gy dose was selected for all our invitro dose to verify the effects. Results were expressed as means ± SD (n=6).

Antioxidants and Redox Signaling
Mitochondria as Target for Tumor Management of Hemangioendothelioma (DOI: 10.1089/ars.2020.8059)

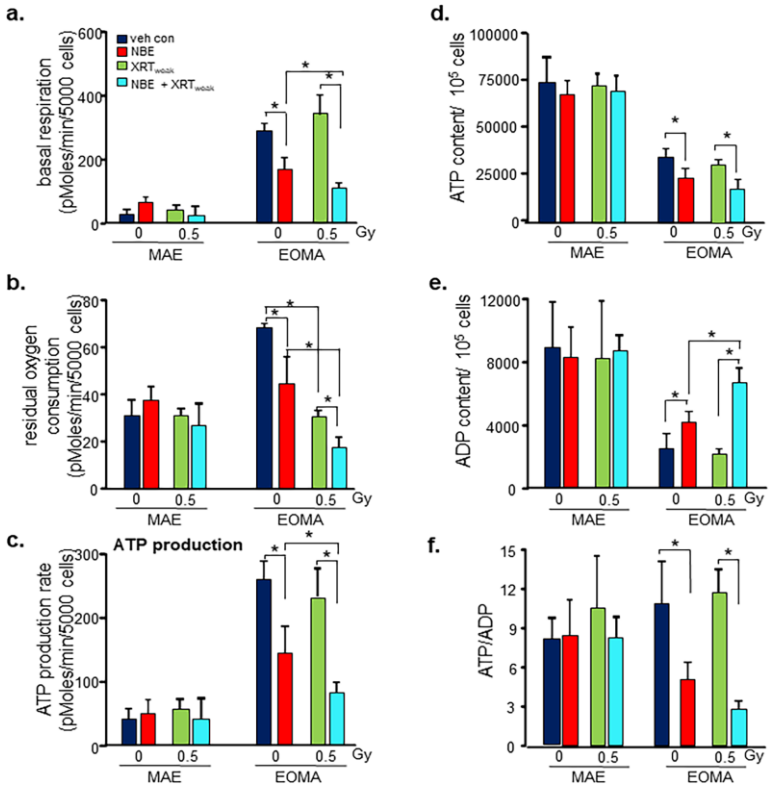

Fig. 4

FIGURE 4

Blunted cellular respiration and reduced ATP production in EOMA cells.

a, Basal respiration measured from Seahorse XF96 was significantly inhibited with weak XRT in NBE treated EOMA compared to MAE. **b**, The residual oxygen consumption also gets compromised with weak XRT exposure in NBE treated EOMA cells. No such effects were observed in non-tumor forming MAE cells. **c**, weak XRT exposure causes decreased rate of ATP production in NBE treated EOMA cells compared to no weak XRT group. All calculations were made using the Agilent Seahorse Software provided with the instrument. Results are expressed as mean ± SD (n = 6). **d**, Basal cellular ATP, ADP (**e**) and the ratio (**f**) were measured in different treatment groups using the EnzyLightTM ADP/ATP ratio assay kit. Results are expressed as mean ± SD (n = 4).

Antioxidants and Redox Signaling
Mitochondria as Target for Tumor Management of Hemangioendothelioma (DOI: 10.1089/ars.2020.8059)

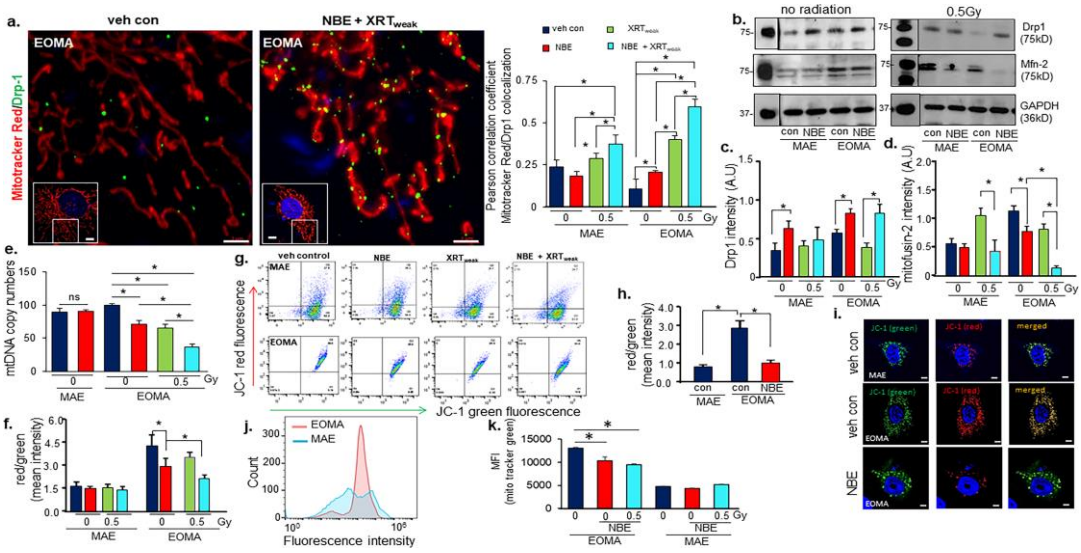

FIGURE 5

Mitochondrial fission and membrane potential.

a, Colocalization analysis of mitochondrial fission marker (Drp1, abcam, ab184247 1:200) and MitoTracker Red CMXRos (250nM) in MAE and EOMA cells before and after treatment of NBE or XRT (n = 3-5)**.** Scale bar = 2 μm. Inset shows the cell from which the region of interest was taken. Scale bar = 5 μm. Complete image set is presented as Sup Fig. 2. **b**, Western blot images of Mfn-2 and Drp-1 protein expressions was compared between no-XRT group and weak XRT exposure in NBE or vehicle treated MAE/EOMA cells. (**c**) Bar graph for Drp-1 and (**d**) Mfn-2 protein expressions, normalized with β-actin. **e**, Mitochondrial copy numbers of MAE and EOMA cells exposed to vehicle control or NBE. In addition, mitochondrial copy numbers determination was done o EOMA cells were further exposed with weak XRT with or without NBE (n = 3). **f**, Loss of mitochondrial membrane potential in EOMA and MAE cells exposed with weak XRT with or without NBE, as assessed by JC-1 flow cytometry. Cells were collected 6h after XRT exposure with or without NBE treatment and stained with 2.5μM of JC-1 for 15mins. The ratio of red to green shows significant decrease of mitochondrial membrane potential in combined treatment of NBE & XRT than XRT alone. Results are expressed as mean ± SD (n = 6). **g,** Representative images of cell populations analyzed by the Flow Cytometer (Beckman-Coulter), using a 488 laser, following standard protocols provided by JC-1 manufacturers. **h,** Intensity calculation and **i,** Representative airyscan confocal (ZEISS LSM 880, Germany) images of cells subjected to JC-1 staining (2.5μM, 30mins) with or without NBE treatment in EOMA cells

compared with untreated MAE cells.**j,** Flow cytometric profiles of mitochondrial mass levels in EOMA and MAE cells after exposed to NBE, by Mito Tracker green FM (25nM). **k**, Median fluorescence intensity (MFI) of Mito Tracker green FM of EOMA and MAE cells exposed with weak XRT with or without NBE.Results are expressed in mean ± SE (n = 6).

Antioxidants and Redox Signaling
Mitochondria as Target for Tumor Management of Hemangioendothelioma (DOI: 10.1089/ars.2020.8059)

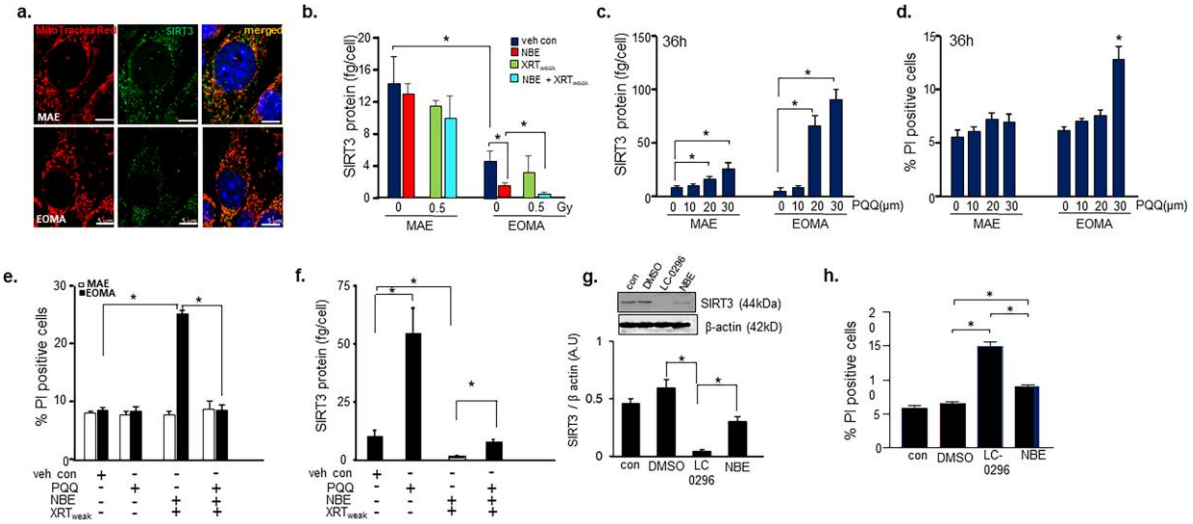

Fig. 6

FIGURE 6

SIRT3 depletion responsible for inducible death of EOMA.

a, Representative image of intracellular SIRT3 localization in MAE, EOMA cells. **b**, EOMA and MAE cells were seeded in equal number (100000 cells/well) in 12 well plate. After the mentioned treatment schedule cells were isolated and measured for SIRT3 level using SIRT3 ELISA kit. SIRT3 levels was normalized to the number of cells seeded per well. Sirt3 levels were significantly reduced in cellular supernatant of EOMA compared to MAE, it was further reduced when treated with NBE alone or combined exposure of NBE and weak XRT in EOMA cells. **c**, Pyrroloquinoline quinone (PQQ), chemical activator of Sirt 3 causes induction of Sirt3 in dose dependent manner in both MAE and EOMA, (**d**) Significant cell death was observed in EOMA cells with 30μM as shown by PI positivity. (**e**) 12h pretreatment with PQQ (20μM) significantly rescued the cellular survival of EOMA cells compared to combined exposure of NBE and weak XRT and subsequently the level of Sirt3 were found to be significantly elevated (**f)** at that point. Results are expressed as mean ± SD (n = 3). (g) Western blot images of SIRT3 protein expression was compared between control, vehicle control (DMSO), LC-0296 (10μM) and NBE treated groups in EOMA cells. Signal intensities of SIRT3 protein is normalized with β-actin. Results are expressed as mean ± SD (n = 3). (h) Percentage of PI fluorescence expressing cells were counted by flow cytometry, after staining NBE and LC-0296 treated EOMA cells with propidium iodide (10μg/ml) using standard protocol. Data are expressed as mean ± SEM (n = 6).

Antioxidants and Redox Signaling
Mitochondria as Target for Tumor Management of Hemangioendothelioma (DOI: 10.1089/ars.2020.8059)

Antioxidants and Redox Signaling
Mitochondria as Target for Tumor Management of Hemangioendothelioma (DOI: 10.1089/ars.2020.8059)

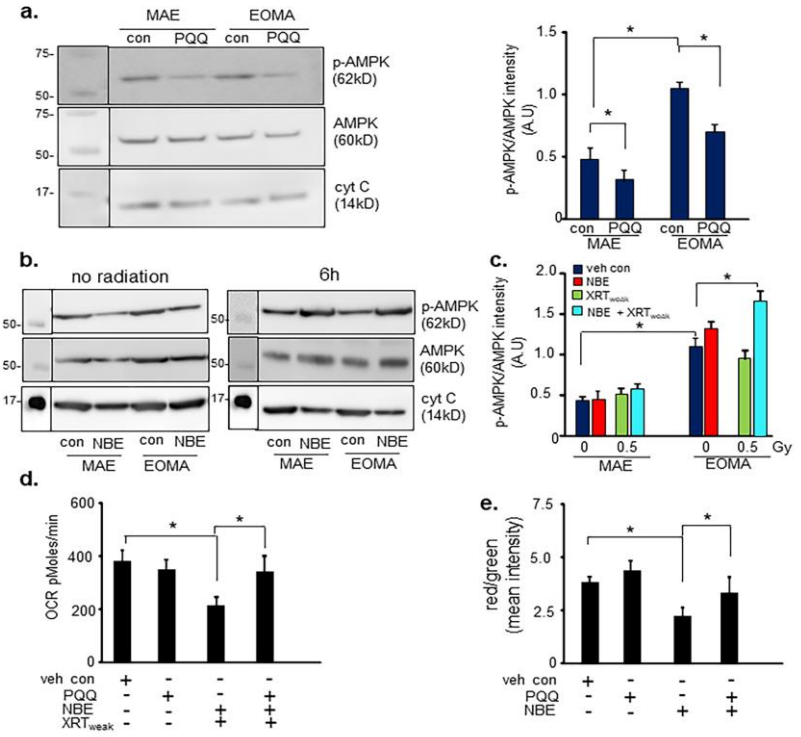

Fig. 7

FIGURE 7

AMPK phosphorylation caused by severe depletion of SIRT3 compromises mitochondrial respiration in EOMA cells.

a, Western blot shows elevated ratio of phospho-AMPK to AMPK in EOMA cells compared to MAE. PQQ treatment reduces the AMPK activation by inhibiting phosphorylation in both MAE and EOMA cells. **b**, Western blot images of phospho-AMPK and AMPK in NBE alone or combined exposure of NBE and weak XRT. **c**, Intensity calculation confirms either NBE alone or in combination with weak XRT increases the phosphorylation of AMPK in EOMA cells. Results are expressed as mean ± SD (n = 3). **d**, OCR data shows, pretreatment with PQQ rescued the combined effect of NBE and weak XRT. Results are expressed as mean ± SD (n = 7).

Antioxidants and Redox Signaling
Mitochondria as Target for Tumor Management of Hemangioendothelioma (DOI: 10.1089/ars.2020.8059)

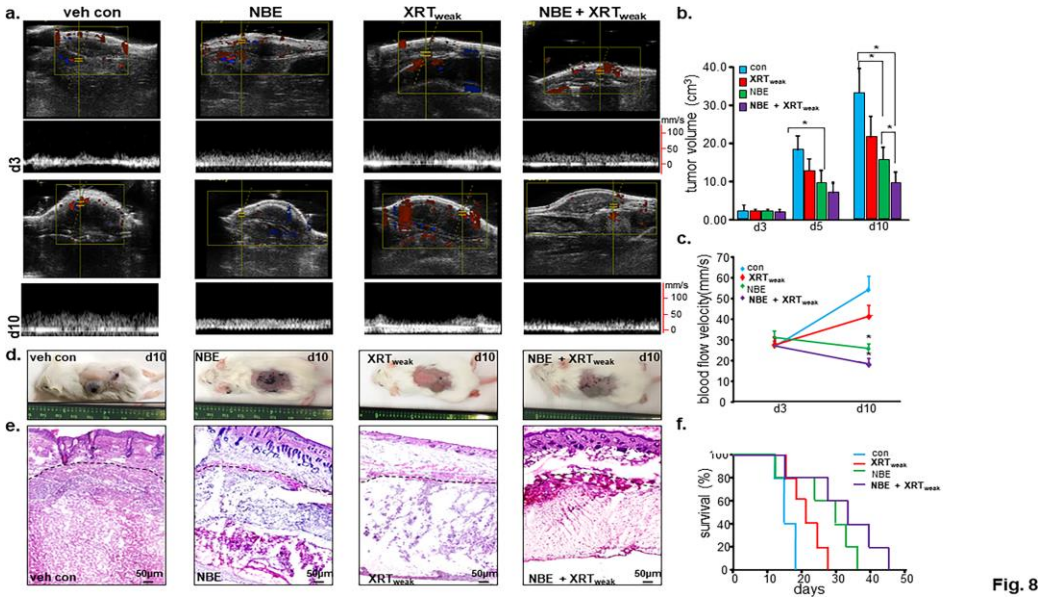

Fig. 8

FIGURE 8

Improved survival of mice with HE tumor.

Syngeneic 6-8 week old female 129 P/3 mice received a subcutaneous injection of EOMA cells. Mice were treated with NBE oral gavage (20mg/kg) and topical application (200mg/kg) once daily. XRT exposure using irradiator RS2000 was carried out with 2.5Gy gamma XRT per dose directed at the tumor given on the 3rd, 5th and 7th day after EOMA cell injection for a total dose of 7.5 Gy. a, ultrasound imaging of animals from each group (n=5) were performed on a Vevo2100 system (Toronto, Ontario, Canada) using high frequency linear array transducers operating between 8 and 17 MHz. b, Tumor volume was quantified using calipers (length x width x height). Significantly reduced tumor growth was observed at day 10 in NBE +XRT treated group compared to others. c, tumor blood flow was analyzed using Vevo2100 system shows significant difference at day 10 after NBE+XRT combined treatment compared to other groups. d, Representative images of tumor in different treatment group. e, H&E staining of tumor section after 10 day of cell injection shows decreased cellular granularity. f, Kaplan-Meier survival curve analyzed by log-rank analysis shows mice treated with vehicle, XRT only, NBE only and NBE + XRT. Results are expressed as mean ± SD (n = 5). Here NBE only and NBE + XRT treatment have a significant survival advantage compared to vehicle control, * $p < 0.05$. Also, NBE + XRT treatment have a significant survival advantage compared to XRT only, * $p < 0.05$.

Antioxidants and Redox Signaling
Mitochondria as Target for Tumor Management of Hemangioendothelioma (DOI: 10.1089/ars.2020.8059)

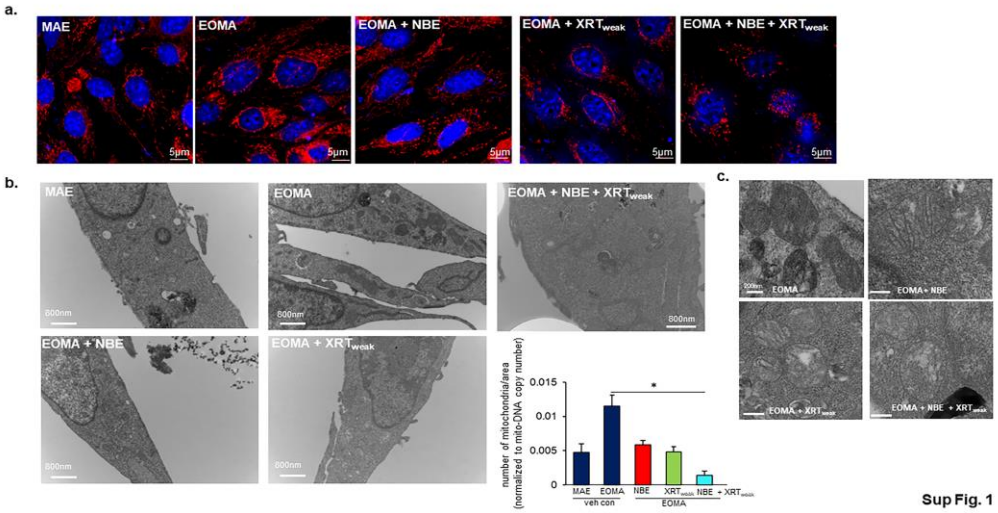

SUPPLEMENTARY FIGURE 1

Decreased mitochondrial abundance after NBE treatment

a, Representative images of cells stained with mitotracker red shows mitochondrial abundance in EOMA compared to MAE. Treatment with NBE and XRT_{weak} changed mitochondrial appereances in EOMA cells. **b**, Transmission electron microscopy observation of the mitochondria in (Top) MAE, EOMA cells and EOMA cells treated with NBE+XRT_{weak}. Bottom panel represent the mitochondrial morphology of EOMA cells before and after treatment of NBE or XRT_{weak}. Bar graph showing the abundance of mitochondria in above-mention conditions normalized with mtDNA copy number. (**c**) Magnified transmission electron microscopy images of the mitochondria as shown in (**panel b**). Top panel represent the mitochondrial morphology EOMA cells and EOMA cells treated with NBE. Bottom panel represent the mitochondrial morphology of EOMA cells treatment of XRT_{weak} alone or XRT_{weak} combined to NBE treatment.

Antioxidants and Redox Signaling
Mitochondria as Target for Tumor Management of Hemangioendothelioma (DOI: 10.1089/ars.2020.8059)

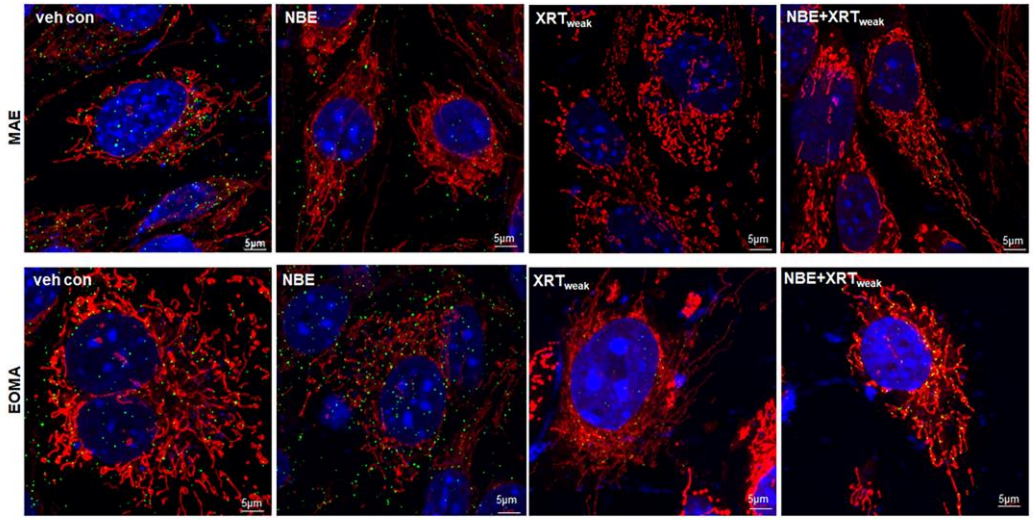

Sup Fig. 2

SUPPLEMENTARY FIGURE 2

Confocal analysis of mitochondrial fission

High-resolution confocal images of mitochondrial fission marker (Drp1) (**green**) and MitoTracker Red CMXRos **(red)** in MAE and EOMA cells before and after treatment of NBE or XRT_{weak}. The quantitation has been provided in Fig. 5a.

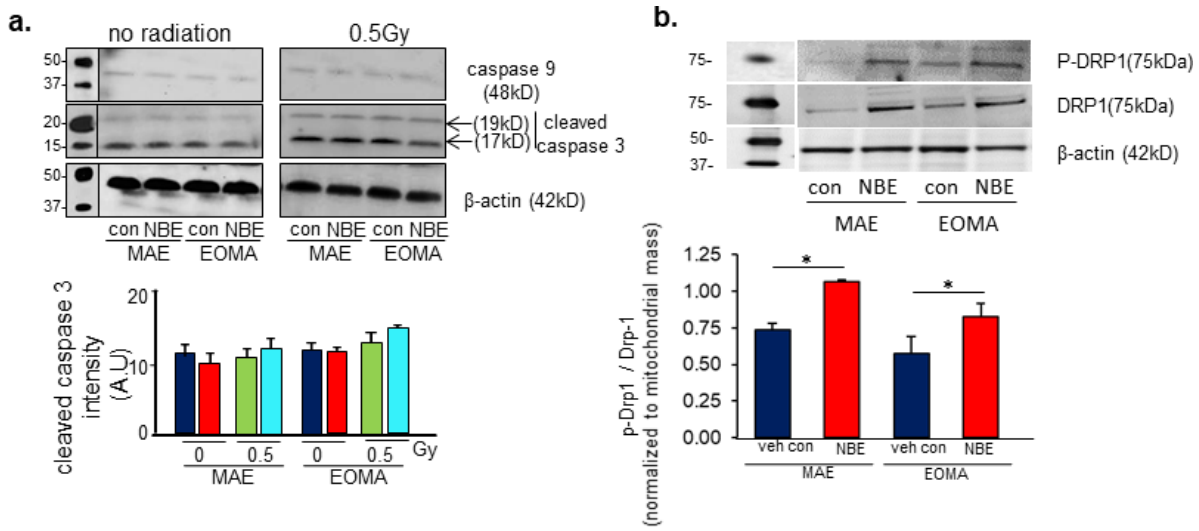

Supplementary figure 3: Induced phosphorylation of DRP-1 with NBE treatment

a, Western blot images of cellular caspase 9 and cleaved caspase 3 protein expression was compared between no-XRT group and weak XRT exposure in NBE or vehicle treated MAE/EOMA cells. Relative bar graph for cleaved caspase 3 protein expressions, normalized with β-actin. Results are expressed as mean ± SD (n = 3). **b**, Detection of P-DRP1 and DRP1 protein expression in NBE or vehicle treated MAE/EOMA cells by Western blot. Signal intensities of P-DRP1/DRP1 protein is normalized with mitochondrial mass. Results are expressed as mean ± SD (n = 3).

Antioxidants and Redox Signaling
Mitochondria as Target for Tumor Management of Hemangioendothelioma (DOI: 10.1089/ars.2020.8059)

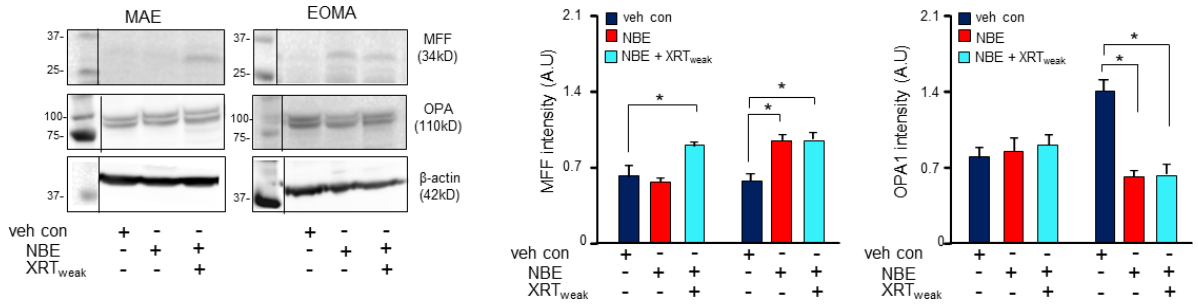

SUPPLEMENTARY FIGURE 4

Additional mitochondrial fission and fusion markers investigation in EOMA and MAE cells.

Mitochondrial fission marker protein, Mitochondrial Fission Factor (MFF) was significantly induced and mitochondrial fusion marker protein, Dynamin-like protein (OPA1) was significantly reduced with NBE and XRT_{weak} treatment in EOMA cells. Results are expressed as mean ± SD (n = 3).

Antioxidants and Redox Signaling
Mitochondria as Target for Tumor Management of Hemangioendothelioma (DOI: 10.1089/ars.2020.8059)